Available online at www.sciencedirect.com
SCIENCE DIRECT
Journal of Molecular Graphics and Modelling 24 (2006) 307–318
Journal of Molecular Graphics and Modelling
www.elsevier.com/locate/JMGM

# Novel properties of malarial *S*-adenosylmethionine decarboxylase as revealed by structural modelling

Gordon A. Wells [a], Lyn-Marie Birkholtz [a], Fourie Joubert [a], Rolf D. Walter [b], Abraham I. Louw [a,*]

[a] *Department of Biochemistry, School of Biological Sciences, Faculty of Natural and Agricultural Sciences, University of Pretoria, Pretoria 0002, South Africa*
[b] *Department of Biochemical Parasitology, Bernhard Nocht Institute for Tropical Medicine, Hamburg, Germany*

Received 2 March 2005; received in revised form 15 September 2005; accepted 29 September 2005
Available online 27 October 2005

**Abstract**

In the malaria parasite, the two main regulatory activities of polyamine biosynthesis, ornithine decarboxylase (ODC) and *S*-adenosylmethionine decarboxylase (AdoMetDC) occur in a single bifunctional protein. The AdoMetDC domain was modeled using the human and potato X-ray crystal structures as templates. Three parasite-specific inserts and the core active site region was identified using a structure-based alignment approach. The domain was modeled without the two largest inserts, to give a root mean square deviation of 1.85 Å from the human template. Contact with the rest of the bifunctional complex is predicted to occur on one face of the *Plasmodium falciparum* AdoMetDC (PfAdoMetDC) domain. In the active site there are four substitutions compared to the human template. One of these substitutions may be responsible for the lack of inhibition by Tris, compared to mammalian AdoMetDC. The model also provides an explanation for the lack of putrescine stimulation in PfAdoMetDC compared to mammalian AdoMetDC. A network of residues that connects the putrescine-binding site with the active site in human AdoMetDC is conserved in the malarial and plant cognates. Internal basic residues are found to assume the role of putrescine, based on the model and site-directed mutagenesis: Arg11 is absolutely required for normal activity, while disrupting Lys15 and Lys215 each cause 50% inhibition of AdoMetDC activity. These novel features of malarial AdoMetDC suggest possibilities for the discovery of parasite-specific inhibitors.


*Keywords:* Homology model; Malaria; Bifunctional; AdoMetDC; Polyamines; Pyruvoyl

## 1. Introduction

*Plasmodium falciparum* is the principal agent responsible for severe malaria. Malaria affects 300–500 million people annually, and kills approximately 2 million [1]. The emergence and spread of *P. falciparum* strains resistant to existing drugs calls for the discovery of new parasite-specific inhibitors. One potential parasite metabolic target is polyamine biosynthesis. The polyamines (putrescine, spermidine and spermine) are a class of polycationic molecules essential for rapidly proliferating cells. Polyamines are thought to stabilize DNA and RNA in vivo [2,3]. Spermidine is required for the synthesis of the translation initiation factor eIF-5A [4,5] and in Trypanosomes for the biosynthesis of the glutathione mimic, trypanothione [6]. The biosynthesis of polyamines therefore appears to be a viable parasite drug target [7]. Polyamine metabolism has already been extensively studied as a potential human cancer target. Success to date has been moderate, generally it is only possible to induce cytostasis [8]. This is thought to be partly due to the short half-lives of the main regulatory enzymes [3,9]. However, one polyamine targeting drug, 2-difluoromethylornithine (DFMO), has already been used to successfully treat African sleeping sickness caused by *Trypanosoma brucei gambiense* [10,11].

Biosynthesis of polyamines is regulated by two enzymes: ornithine decarboxylase (ODC, EC 4.1.1.17), and *S*-adenosylmethionine decarboxylase (AdoMetDC, EC 4.1.1.50). ODC produces putrescine by decarboxylation of ornithine. Putrescine then serves as a scaffold for the further addition of aminopropyl groups to form the main polyamines spermidine

* Corresponding author. Tel.: +27 12 420 2480; fax: +27 12 362 5302
*E-mail address:* braam.louw@bioagric.up.ac.za (A.I. Louw).

1093-3263/$ – see front matter 
doi:10.1016/j.jmgm.2005.09.011

and spermine. The aminopropyl groups are donated by decarboxylated *S*-adenosylmethionine, the product of AdoMetDC.

In all eukaryotes studied so far, excepting *P. falciparum*, ODC and AdoMetDC activities occur in separate proteins. In *P. falciparum*, both activities are present in one protein of 1419 residues. AdoMetDC activity is found within the first 570 residues of the N-terminal region, while ODC activity resides in the C-terminal region [12,13]. The two domains are connected by a linker region of about 100 amino acids. The reason for this bifunctionality is as yet unclear, as the two enzyme activities can function independently [13], but there are nonetheless cross-domain interactions [14]. The evolutionary advantage to the parasite may simply lie in its being able to regulate polyamine biosynthesis through the abundance of one protein [13]. This unusual arrangement of the two functions in a single protein provides an attractive target for the discovery of parasite-specific drugs.

Unlike most decarboxylases which require pyridoxal phosphate as cofactor, AdoMetDC is a member of a small class of enzymes that utilize pyruvoyl instead. Pyruvoyl is generated internally from a serine residue during an autocatalytic, non-hydrolytic cleavage. Current biochemical evidence indicates that pyruvoyl acts as an electron sink during the decarboxylation reaction by allowing the carboxyl moiety to act as a leaving group [15–18].

In some organisms the activity and/or proteolytic processing of AdoMetDC is stimulated by putrescine. In humans both activity and processing are stimulated [19], whereas in certain fungi this effect has only been observed on activity [20]. The effect on processing has however been given less attention. Stimulation is generally not observed in parasites, or only at much higher concentrations of putrescine. In the case of plants [21] and *P. falciparum* [13] no stimulation of activity is observed.

Eukaryotic AdoMetDC comprises an αββα sandwich, with the active site located between the β-sheets [17,22]. Autoproteolytic cleavage generates the shorter N-terminal β-chain (about 9 kDa) and the longer C-terminal α-chain (about 160 kDa). In mammals AdoMetDC functions as a dimer, mediated by an edge-on association of the β-sheets. In humans one putrescine binds each monomer in an allosteric site 15–20 Å from the active site [23]. In *P. falciparum*, the bifunctional protein also associates to form a dimer, yielding a hetero-tetramer after cleavage [12].

This paper provides insights into the structural features of PfAdoMetDC. Based on this model and site-directed mutagenesis, a putrescine independent mechanism of stimulation is proposed. The novel properties uncovered will guide further validation studies of AdoMetDC model and its development as a target for parasite-specific inhibitors.

## 2. Methodology

### 2.1. Alignment

Alignment was carried out with Clustalx 1.81 [24]. The alignment used for modeling was created using the Gonnet set of matrices, with gap-opening and gap-extension penalties of 15 and 0.31, respectively. The delay divergent sequences property was set to 20%, and negative matrices used. Due to the low sequence identity between the AdoMetDC sequence from *P. falciparum* compared to those of the template a number of strategies were applied to increase confidence in the alignment. Firstly, sequences for the complete bifunctional protein from the rodent malarial parasites *P. yoelii* and *P. berghei* [14], and partial sequences for *P. chaubaudi* and *P. knowlesi* (Unpublished results) were included. This was to increase the chances of correctly distinguishing conserved AdoMetDC core regions from *Plasmodium*-specific inserts. In order to remove the bias introduced by the five *Plasmodium* sequences, a large number of sequences from other eukaryotes were used. Secondly, conserved motifs were identified in the same set of sequences with MEME 3.0.3 [25]. The alignment was then adjusted in order to reflect high scoring motifs that were not found during the initial alignment. Care was taken not to introduce disruptions in α-helices and β-strands according to the human [17] and potato [22] structures of AdoMetDC. Finally, the alignment was verified using about 20 secondary structure prediction algorithms on the full length *Plasmodium* sequences.

The full list of sequences used (Swissprot accession numbers in brackets): *Bos taurus* (P50243), *Homo sapiens* (P17707), *Mesocricetus auratus* (P28918), *Mus musculus* (P31154), *Rattus norvegicus* (P17708), *Xenopus laevis* (P79888), *Drosophila melanogaster* (P91931), *Caenorhabditis elegans* (O02655), *Onchocerca volvulus* (Q27883), *Leishmania donovani* (Q25264), *Trypanosoma brucei brucei* (P50244), *Trypanosoma cruzi* (O76240), *Arabidopsis thaliana* (Q96286), *Brassica juncea* (Q42613), *Catharanthus roseus* (Q42679), *Datura stramonium* (Q96555), *Dianthus caryophyllus* (Q39676), *Helianthus annuus* (O65354), *Hordeum chilense* (Q42829), *Zea mays* (O24575), *Nicotiana sylvestris* (O80402), *Oryza sativa* (O24215), *Pisum sativum* (Q43820), *Pharbitis nil* (Q96471), *Solanum tuberosum* (Q04694), *Spinacia oleracea* (P46255), *Nicotiana tabacum* (O04009) and *Saccharomyces cerevisiae* (P21182).

### 2.2. Homology modeling

The AdoMetDC crystal structures of the potato enzyme (2.3 Å, PDB entry 1 MHM: Ref. [22]) and the human enzyme irreversibly complexed with the substrate methyl-ester (1.9–2.7 Å, PDB entry 1I7B: Refs. [17,23] were used as templates for homology modeling. Initial models were built with Modeller 6v2 [26–28], using a high refinement (refine_4) to generate 100 models. The modified pyruvoyl residue was modeled by manually editing the Modeller library files. From this set one model was chosen for further analysis based on Ramachandran plots [29]. After superimposition with the human template, the irreversibly bound methyl ester of the substrate (MeAdoMet) was transferred to this model. Hydrogens were added in InsightII (Accelrys) at a pH of 7.2. Heteroatom bonds of the ligand and pyruvoyl residue were manually adjusted to accurately reflect the chemical nature of the ligand. Minimization was performed in InsightII/Discover3 with the

Table 1
PfAdoMetDC/ODC mutation primers[a]

| Mutation | Primers | 5′ → 3′ |
|---|---|---|
| Arg11Leu | Forward | GGA-ATT-GAA-AAA-*TTA*-GTT-GTG-ATC-AAA-TTA-AAG-G |
| | Reverse | C-CTT-TAA-TTT-GAT-CAC-AAC-*TAA*-TTT-TTC-AAT-TCC |
| Lys15Ala | Forward | GG-GTT-GTG-ATC-*GCA*-TTA-AAG-GAG-AG |
| | Reverse | CT-CTC-CTT-TAA-*TGC*-GAT-CAC-AAC-CC |
| Lys215Ala | Forward | GCT-TCT-ACG-TTT-*GCA*-TTC-TGT-TCG-G |
| | Reverse | C-CGA-ACA-GAA-*TGC*-AAA-CGT-AGA-AGC |

[a] Mutations are indicated in italics.

cff91 forcefield. A cutoff of 9.5 Å was used for van der Waals and electrostatic interactions with a distance dependent dielectric constant of 4. Energy minimization was carried out in two phases. The first phase comprised steepest descent minimization to a maximum derivative of 1000 kcal $mol^{-1}$. In the second phase conjugate gradients were used to minimize to 1 kcal $mol^{-1}$. Results of modeling were analyzed using Procheck [30], Ligplot 4.1.1 [31], Cerius2 (Accelrys) [32] and Pymol (http://www.pymol.org). The DSSP algorithm [33] was used to assign secondary structure as implemented in the DSSPCMBI program (version April 1, 2000).

### 2.3. Lack of putrescine stimulation

Reasons for the lack of putrescine stimulation of PfAdoMetDC were investigated. MeAdoMet was added as described above to the initial unminimized model. A chimeric model was generated in order to mimic the human putrescine-binding site. The following mutations were introduced: Lys215Asp and 11-RVVIK-15 → 11-LVEIW-15. This latter mutation replaces R×V×K in the original sequence with L×E×W. Rotamer studies demonstrated these mutations were made in an energetically favorable conformation. Putrescine was inserted into the putative binding site of each model, via superimposition with the human template including putrescine. Hydrogens were added to the amine moieties of putrescine to produce a dicationic molecule. Energy minimization was carried out on each of these models, as above until a maximum derivative of 1 kcal $mol^{-1}$ was reached. Putrescine was then docked with the SA-Docking module of InsightII. A binding set within 6.5 Å of putrescine was selected. Except for using a set of 30 initial putrescine conformations for each model, the default parameters were used. Binding energies were calculated with the cff91 forcefield.

### 2.4. Effect of putrescine-related mutations

Based on the model three residues possibly related to the lack of putrescine stimulation were chosen for site-directed mutagenesis. The chosen mutations were Arg11Leu, Lys15Ala and Lys215Ala. The primers used for mutagenesis are listed in Table 1. The wild-type bifunctional gene was previously cloned [12,13] into the pASK-IBA3 expression vector (Institut für Bioanalytik, Gttingen Germany). Site-directed mutagenesis was carried out according to the protocol of the QuikChange® mutagenesis kit (Stratagene®). PCR was as follows: initial incubation at 95 °C for 30 s, followed by 18 cycles at 95 °C for 30 s, 55 °C for 1 min and 68 °C for 15 min. Each reaction (50 μl) contained 50 ng of plasmid, 125 ng each of forward and reverse primers, 2 mM of each dNTP and 6 U of *Pfu* polymerase (Promega®, USA). After PCR the mixture was incubated with *Dpn* I (40 U, New England Biolabs) for 2 h at 37 °C. Mutant plasmids were transformed into competent DH5 α *E. coli*. Mutations were confirmed using the Big Dye® automated sequencing kit version 2.0 in an ABI 377® Automated Sequencer (Applied Biosystems, USA).

Protein expression was performed using the Strep-tag II fusion-protein system (Institut für Bioanalytik) as previously described [34]. Briefly, wild-type and mutant PfAdoMetDC/ODC constructs were separately expressed in ODC- and AdoMetDC-deficient EWH331 *E. coli* [35]. One colony was grown to saturation in Luria–Burtani (LB) medium with 0.05 g $ml^{-1}$Ampicillin (Amp) at 37 °C, then diluted 1:10 in LB-Amp and grown at 37 °C to an $A_{600}$ of 0.5 units. Expression was induced with anhydrotetracycline (0.2 μg $ml^{-1}$, Institut für Bioanalytik), and the cultures shaken overnight at 22 °C. Cells were harvested by pelleting, and the pellets resuspended in 20 ml 1 M Tris–HCl, 1 mM EDTA, pH 8.0. Cell contents were released by lysozyme digestion followed with sonication, and the cell debris removed by ultracentrifugation (100,000 *g*, 1 h, 4 °C). The recombinant protein was purified according to manufacturer instructions. Protein concentrations were determined by Bradford assay [36]. Expression was followed by SDS-PAGE with Coomasie Blue staining. AdoMetDC activity was determined by trapping of $^{14}CO_2$ from *S*-adenosyl-L-[methyl- $^{14}C$] methionine (58 mCi $mmol^{-1}$, Amersham Pharmacia Biotech) as previously described [12]. Duplicate assays were performed for each of two time points to confirm linearity (15 and 30 min), yielding four specific activities for a protein extract. The effect of the mutations on enzyme processing was followed by SDS-PAGE.

## 3. Results

### 3.1. Sequence properties

The AdoMetDC domains of *Plasmodium spp*. are highly divergent from that of other eukaryotic enzymes and have *Plasmodium*-specific inserts. In order to optimize the sequence alignment, a structure-based approach was followed. During

the course of modifying alignment parameters, the frequency with which secondary structural elements of the human template were matched with the same region in the *P. falciparum* sequence was monitored. This semi-quantitative analysis of the similarity of the various secondary structure elements of the human structure reveals that the more conserved elements surround the active site, while the more divergent elements cluster on one side of the protein. This prompted the inclusion of AdoMetDC from other *Plasmodium* species. After this inclusion, elements with low similarity, which initially proved difficult to identify within the *P. falciparum* sequence, were easier to find (Fig. 1). To further increase confidence in the alignment, manual corrections were made using conserved motifs as identified by MEME. Finally, the alignment of secondary structural regions in the template confirmed secondary structure predictions in the *Plasmodium* sequences.

Initial studies suggested the presence of one large insert in PfAdoMetDC [12,14]. However, during the course of creating multiple alignments, three inserts became apparent. The positions of the inserts are indicated in Fig. 2.

The following manual adjustments were made to prevent disruption of secondary structural elements: Insert 1 of PfAdoMetDC was moved two residues downstream to run from Lys57 to Glu63, to prevent a insertion within β-strand 2 (Initial alignments correctly identified β-strand 2, however, there was some ambiguity regarding its C-terminus). Insert 1 is 7 residues long and occurs in all *Plasmodium* species with known sequences, with 43% similarity between *P. falciparum* and the other *Plasmodium* sequences. Insert 2 (Val110-Lys137) was moved five residues upstream to prevent a disruption within a second β-strand. Insert 2 consists of 27 residues, with a higher degree of similarity (about 50% for *P. falciparum*), and a similar distribution of hydrophobic and polar residues. Due to the difficulties of reliable de novo modeling of long loops [28], the majority of insert 2 was excised, leaving overhangs of two residues. The region corresponding to human α-helix 6 and the four preceding residues was moved five residues downstream according to the results of motif identification. This resulted in the region corresponding to β-strand 7 being shifted downstream one residue. The regions corresponding to α-helices 8 and 9 were manually adjusted in order to minimize the number of inserts, making insert 3 about 150 residues long.

Insert 3 is the most divergent, being about 250 residues in the rodent parasites (*P. berghei*, *P. yoelii*). As for insert 2, the majority of insert 3 was excised. The regions corresponding to human β-sheets 15 and 16 were manually adjusted to maximize alignment of hydrophobic residues.

### 3.2. Model properties

The topology of the final minimized model and the templates is similar (Fig. 3), adopting the same αββα-fold as for human and potato AdoMetDCs [17,22]. The root mean square deviation (RMSD) of the backbone $C_\alpha$ atoms between the unminimized model and templates were 1.45 and 1.64 Å for the human and potato templates, respectively. Minimization (1219 steps) resulted in a slightly poorer Ramachandran plot, with a decrease in residues found in most favored regions, from 87 to 74% (Fig. 4). The final RMSD with the human template is 1.85 Å. A similar increase in RMSD between the model and potato template (1.64–2.22 Å) occurred. The total change in energy during minimization was $3.6 \times 10^5$ kcal mol$^{-1}$(final energy: −5664.8 kcal mol$^{-1}$). The number of residues found in generously allowed and disallowed regions remained constant. Most residues in disallowed regions occurred either in loops or turns, with the exception of Arg249 at the end of helix 8, which occurs in a region of low similarity (Fig. 3). The model has the same number of strands as the human template. There are differences in the number of $3_{10}$-helices and α-helices, however. The model comprises two β-sheets of eight strands each, and two layers of helices. The helix layer adjacent to the β-sheet with the pyruvoyl residue (β-strands 3 & 4) comprises five helices, while the other helix layer comprises six helices. $3_{10}$-helix 5 from the human structure has no counterpart in the malarial model, which is predicted as a random coil instead.

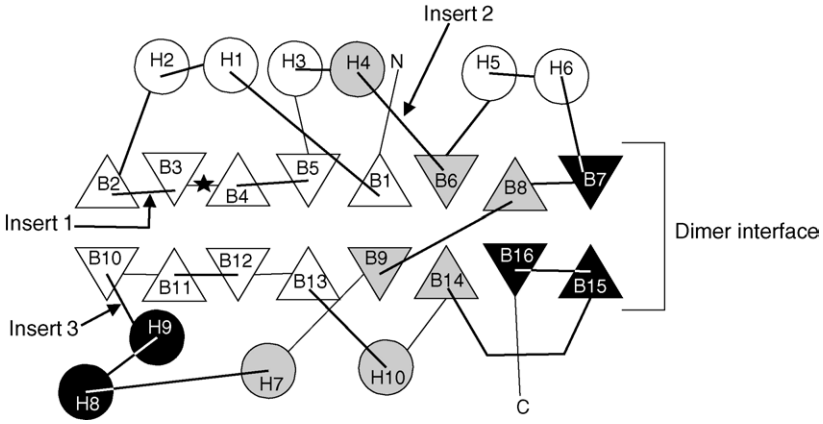


Fig. 1. Conservation of human AdoMetDC secondary structural elements in the *Plasmodium falciparum* sequence. β-strands are represented by triangles, and $3_{10}$- and α-helices by circles. Unshaded: elements, which were easy to identify in the *P. falciparum* sequence. Gray: elements were difficult to identify prior to inclusion of the other *Plasmodium* sequences. Black: elements that remained difficult to find consensus for. The star indicates the site of internal cleavage. Diagram adapted from that of Ekstrom et al. [17]. The relative positions of parasite-specific inserts, and the region that associates for dimer formation in the human enzyme are indicated.

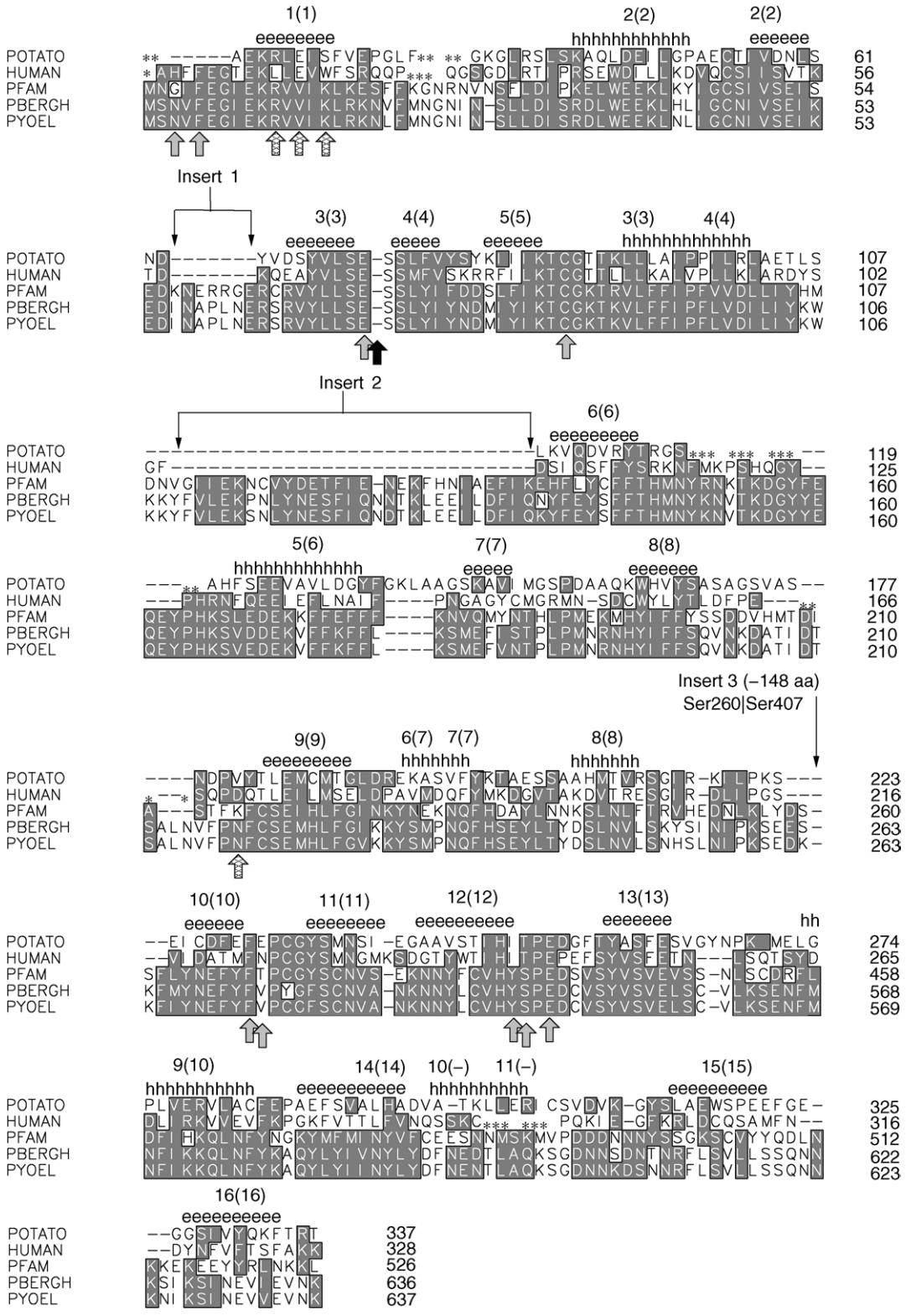


Fig. 2. Target (PFAM) and template alignment used for homology modeling. Similar and identical residues are indicated by shaded boxes. Target sequence chain breaks in gapped regions correspond to excised inserts. Asterisks indicate unresolved residues in the human and potato templates. Helical (h) and sheet (e) regions in the model are indicated. Numbers before brackets correspond to the PfAdoMetDC model, numbers in brackets refer to the corresponding element in the human structure. The number of residues excised for insert is indicated. *Plasmodium berghei* (PBERG) and *Plasmodium yoelii* (PYOEL) sequences are also included. See also Figs. 1 and 3. Key active site residues are indicated by grey and black (pyruvoyl) arrows (see Fig. 5). Residues associated with putrescine stimulation are indicated by cross-hatched arrows (see Figs. 6 and 7).

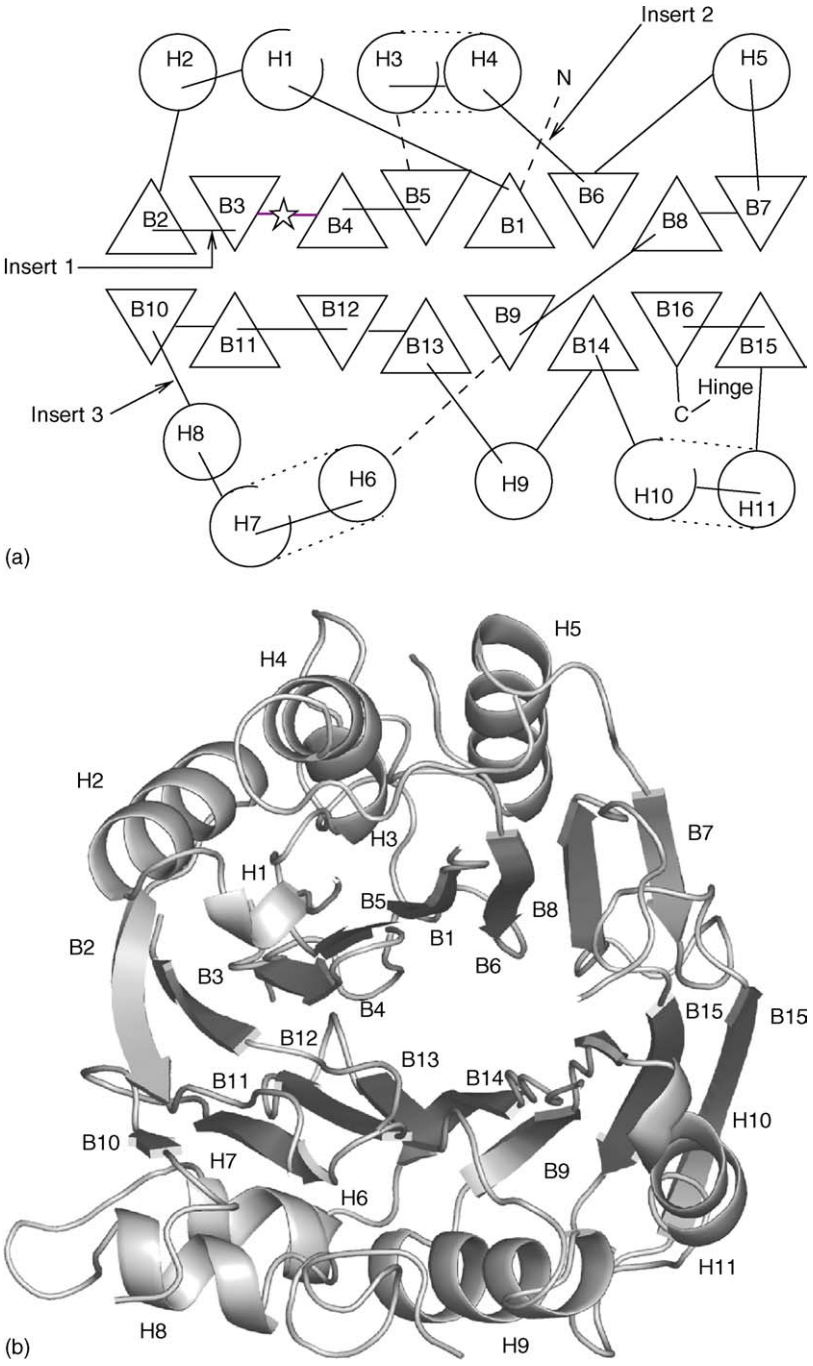


Fig. 3. Topology of the final model. (a) Topology diagram, closed circles: α-helices, open circles denote: 3–10 helices, triangles: β-strands, dashed lines: 3–10 helix contiguous with an α-helix, star: site of proteolytic cleavage/active site. The positions of parasite-specific inserts are indicated. (b) Cartoon diagram of PfAdoMetDC model.

The N-terminus of this helix begins with a Pro, which is conserved in all organisms except *Plasmodium*. The absence of a Pro in PfAdoMetDC should confer increased flexibility, hence the random coil prediction. An extra helical region is present in the non-pyruvoyl αβ-slice of the model comprising a $3_{10}$-helix contiguous with an α-helix (helices 10 and 11).

The model secondary structural elements superimpose well with those of the templates. The more conserved elements superimpose better, except strands 10 and 11. More deviations are seen in regions where homology was difficult to ascertain: helices 8 and 9, and β-strands 15 and 16. Compared to the β-strands, α-helices show more deviation. The active sites superimpose well for β-strands 5, 12 and 13. There is a slight shift of 1-1.5 Å for β-strands 3, 4, 11, and the MeAdoMet ligands.

### *3.3. Active site characteristics*

In the active site all conserved residues show a similar orientation to the human template. Some of the more important

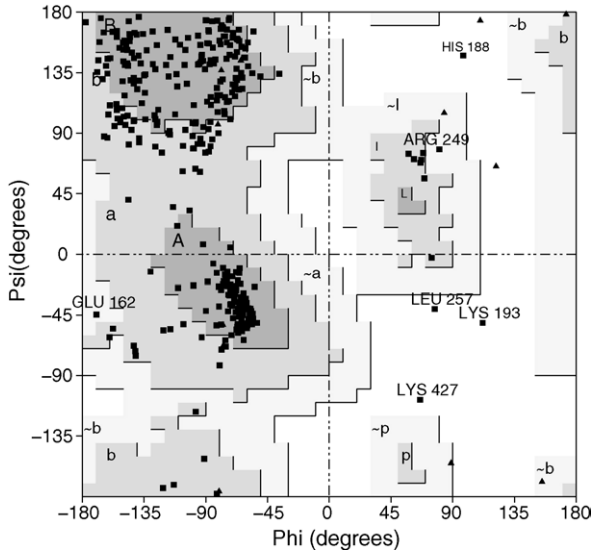


Fig. 4. Ramachandran plot of the PfAdoMetDC model. Most sterically favored regions (dark gray), additional allowed regions (gray), generously allowed regions (light gray), disallowed regions (white). α-helix (A), β-sheet (B), left-handed-helix (L).

residues are shown in Fig. 5. Cys82 *hum(an)* is catalytically important in the human enzyme, and most likely required for protonation of the α-carbon of the substrate cysteinyl moiety after decarboxylation [16]. The sulfhydryl group of this residue, and that of Cys87 points towards the bound inhibitor, while that of Cys87 *pot(ato)* is orientated away. A similar observation is made for Glu72 *pot* which is more embedded within the active site pocket, while Glu72 and Glu67 *hum* lie further out as a result of the presence of the bound inhibitor.

Although the entire malarial sequence shows considerable divergence from other eukaryotes, there are only four substitutions in the active site and surrounding surface (Fig. 5). Important interactions between the human enzyme and the substrate analogue are conserved in the model. The adenine ring of MeAdoMet is stacked hydrophobically between the phenyl rings of Phe5 and Phe415, as in the human structure (Phe7 *hum* and Phe223 *hum*). Mutagenesis of the human enzyme suggested these residues are important for substrate and inhibitor binding [23]. Glu438, like Glu247 *hum*, forms two hydrogen bonds with both hydroxyls of the ribose moiety. In both the model and the human structure there exists a hydrogen bond between $N^1$ of the adenine ring and the amide nitrogen of corresponding Glu residues (Glu67 *hum*, Glu72). The orientation of MeAdoMet within the active site is similar in the model and human structure.

There are similar but less binding interactions with the methyl-ester substrate analogue. Thr245 *hum* is replaced by Ser436. While Thr245 *hum* makes hydrophobic contact with the inhibitor, no interactions are observed for Ser436. Adjacent to this position, Ile244 *hum* is replaced by Tyr435 in *P. falciparum*. Near the mouth of the active site Asn224 *hum* is replaced by Thr416 in *Plasmodium*, and Gly3 replaces His5 *hum*. The latter histidine is about 2 Å closer to MeAdoMet.

In the model, the pyruvoyl residue demonstrates more out-of-plane distortion than the template structures. It is expected that the four atoms of the two carbonyl moieties of pyruvoyl will remain in plane in order for pyruvoyl to act as an electron sink during catalysis. The sulfonium-methyl group displays a slightly different orientation in the model: in the human crystal structure it points towards Tyr193 *hum* of β-strand 11, while in the model it points between Tyr435 of β-strand 12 and Tyr443 of β-strand 13. Surface analysis of the active site reveals a cavity near the sulfonium-methyl moiety of the ligand. In both the model and human the cavity is described by a tyrosine (Tyr252 *hum*, Tyr443) and a glutamate residue (Glu11 *hum*,

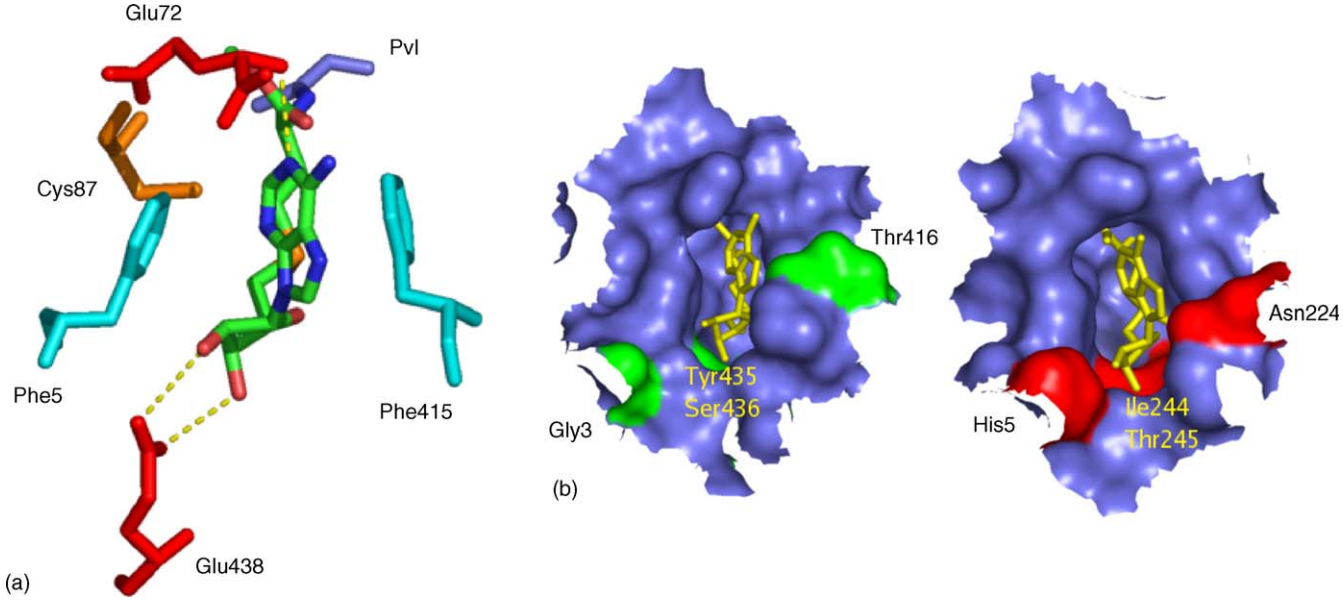


Fig. 5. (a) Important active site residues. Acidic residues (red), aromatic (cyan), polar (orange), modified (slate). Pvl: pyruvoyl. The ligand (MeAdoMet) is colored by atom: N (blue), O (red), C (green), S (orange). Hydrogen bonds are indicated by yellow dashed lines. (b) Substitutions in the model active site. Van der Waals surfaces of the model (left) and human (right) active sites are shown. Substituted residues are indicated (green: model, red: human), and the MeAdoMet ligand (yellow).

Table 2
Residues associated with putrescine stimulation[a]

| Human | Model | Human | Model | Human | Model |
|---|---|---|---|---|---|
| Glu11 | Glu9 | *Asp174* | *Lys215* | *Thr176* | *Cys217* |
| Lys80 | Lys85 | *Leu13* | *Arg11* | *Phe285* | *Tyr478* |
| Glu178 | Glu219 | *Glu15* | *Val13* | *Ser109* | *Tyr142* |
| Glu256 | Glu447 | *Trp17* | *Lys15* | | |

[a] Substitutions/differences between species are indicated in italics.

Glu9). The glutamate residue is conserved across all species, and is situated between 8 and 9 Å from the positive sulfonium atom.

### 3.4. Lack of putrescine stimulation

A number of residues have been implicated in putrescine stimulation of the human enzyme activity and processing. Residues proposed to connect the putrescine-binding site with the active site [18,22] are conserved in the model, human and potato structures (Table 2, Fig. 6). Specifically, Glu11 *hum* in the active site is thought to be connected to the putrescine-binding site via Lys80 *hum*, which in turn is in close proximity to Glu178 *hum* and Glu256 *hum*. A similar arrangement of basic and acidic residues is present in the potato crystal structure [22] and the PfAdoMetDC model. However, some residues that constitute the human putrescine-binding site are substituted in the model (Table 2). In the region of each putrescine amine terminal, basic residues can be observed: Arg11 and Lys15 approximately occupy the region of one terminal each, and Lys215 occurs near Lys15.

In order to elucidate the lack of putrescine stimulation for the *P. falciparum* enzyme, putrescine was docked in a binding site defined by superimposition with the human structure. In the human enzyme the binding site of putrescine is lined with acidic residues that can interact with the positive amine terminals of putrescine (Glu15, Asp174, Glu178 and Glu256). The requirement of these residues for putrescine mediated effects has been confirmed by site-directed mutagenesis [19]. The docking was repeated for a human/*Plasmodium* chimeric model that more closely resembled the human structure (Fig. 7). There is a marked difference in the value of the intermolecular binding energies of putrescine in the chimeric (Lys215Asp and 11-RVVIK-15 → 11-LVEIW-15) and wild-type PfAdoMetDC models. The lowest predicted binding energy for the chimeric model is −853.231 kcal $mol^{-1}$, while that for the unmutated model is −498.808 kcal $mol^{-1}$, suggesting a more favorable interaction in the chimeric model. The orientation of the lowest energy putrescine structures within the mutated model is similar to that in the human template, with the aliphatic backbone running parallel to the β-strands. In contrast, the lowest energy structures of the unmutated model were all orientated 45°−90° to the β-strands. The chimeric model also displayed less backbone deviation than the unmutated wild-type models from the templates.

The potential for internal residues to assume the function of putrescine was established by site-directed mutagenesis. Three

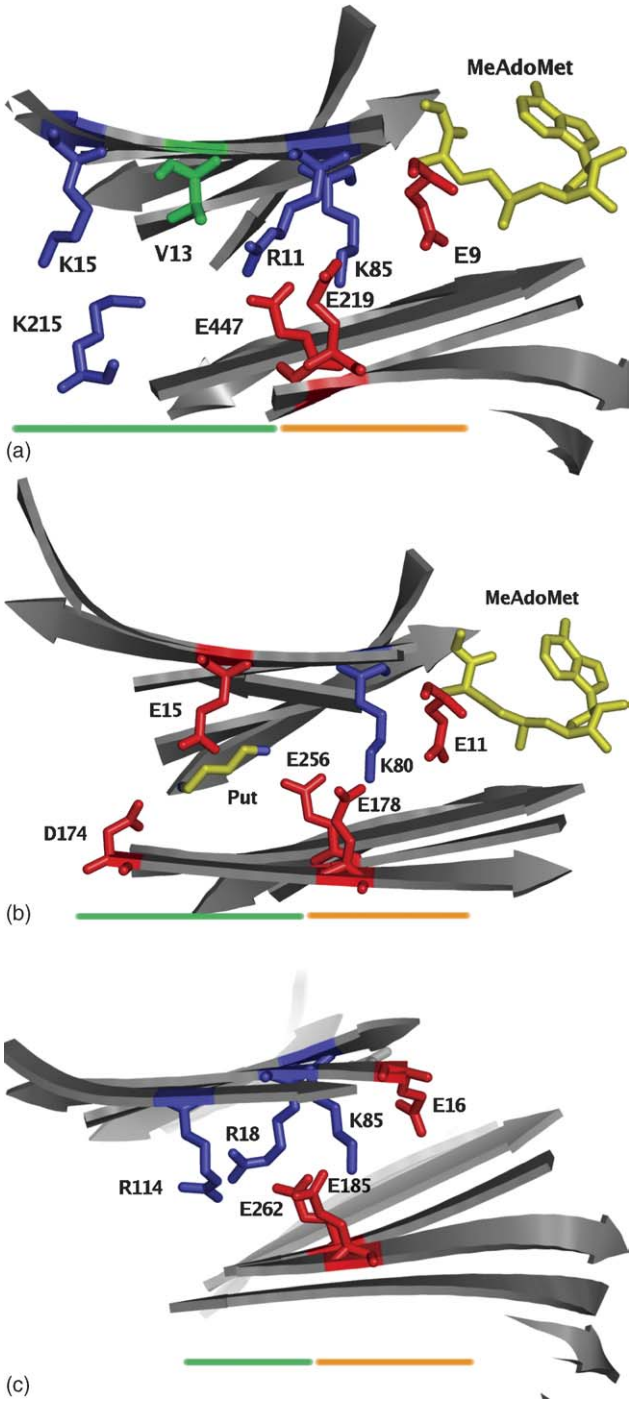


Fig. 6. Important putrescine-related residues. (a) *P. falciparum* model. (b) Human. (c) Potato. Acidic (red), basic (blue), hydrophobic (green) residues, MeAdoMet (yellow) and putrescine (yellow/blue) are indicated by stick models. The orange underlines conserved residues, while the green bar underlines residues that differ across the species.

mutants were made in recombinantly expressed PfAdoMetDC/ODC: Arg11Leu, Lys15Ala and Lys215Ala. The Arg11Leu mutant resulted in an almost inactive protein, as well as an unprocessed protein (Results not shown). The Lys15Ala and Lys215Ala mutants tended to be less active compared to the wild-type, each inactivating PfAdoMetDC by about 50% (Fig. 8).

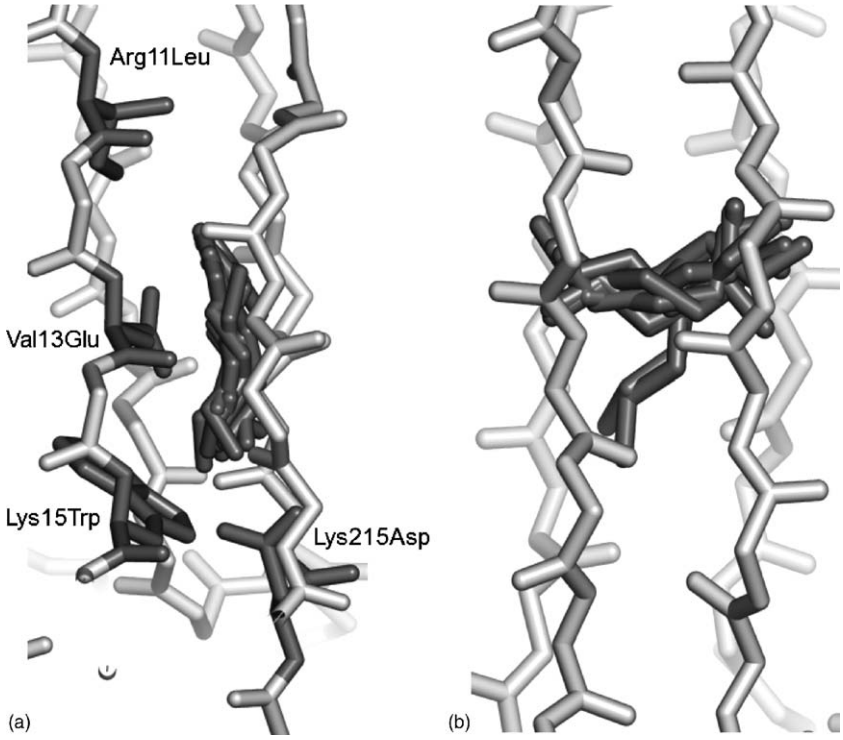


Fig. 7. Orientation of putrescine. (a) Chimeric and (b) wild-type models. The ten best (lowest energy) conformations of putrescine (dark gray) are shown for each. Side chains are also indicated for *in silico* mutations for the chimeric model (dark gray).

## 4. Discussion

The two most important enzymes for regulating polyamine metabolism occur in a single bifunctional enzyme in *Plasmodium* spp. The polyamines are required by organisms in a state of rapid proliferation, and hence represent a potential target in *Plasmodium*, the cause of malaria [10,6]. Knowing the 3D structure of these enzymes could guide the identification of novel inhibitors. The possibility for novel inhibitors is increased if the parasite target has specific features not found in the host. In this study a structure for the AdoMetDC domain of the bifunctional PfAdoMetDC/ODC was produced by homology modeling, which reveals a number of novel properties.

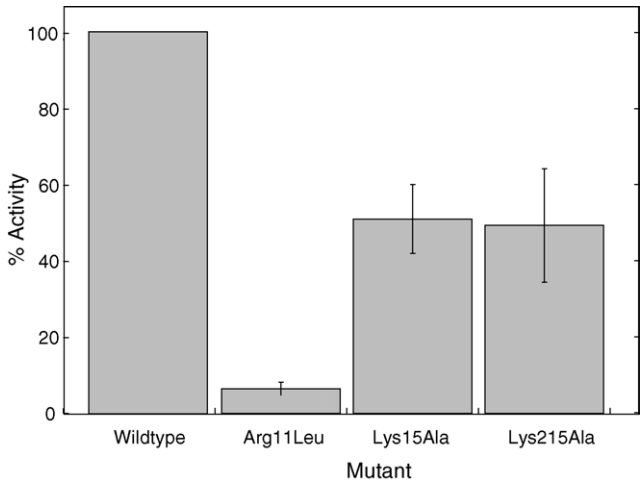


Fig. 8. Effect of mutations on PfAdoMetDC activity. The specific activity was calculated for each mutant, and is presented relative to the wild-type activity (normalized to 100%) from each assay.

Previous studies have established that PfAdoMetDC is a eukaryotic AdoMetDC [12]. Primary structures with low sequence identity can still adopt a similar fold [37]. It is therefore reasonable to expect that PfAdoMetDC will have a similar structure to AdoMetDC from humans and plants. Therefore, to overcome the low sequence identity between PfAdoMetDC and the templates, a strategy was adopted that increased confidence in the alignment at each step. By using sequences from other *Plasmodium* species, motif identification, and secondary structure predictions a credible alignment suitable for homology modeling could be obtained.

Compared to the monofunctional human AdoMetDC, PfAdoMetDC will undoubtedly undergo more protein–protein interactions in the bifunctional complex. This transition to a more protein rich environment should manifest itself in lower sequence identity with the template for those regions undergoing new interactions. The distribution of least conserved elements suggests that one face of PfAdoMetDC undergoes the majority of these interactions (Fig. 1). In the C-terminus of the AdoMetDC domain, β-strands 7, 15 and 16, correspond to the region responsible for dimerization in the human enzyme. It is likely that the same regions in PfAdoMetDC interact in the bifunctional complex, since this would represent a parsimonious evolutionary route. In PfAdoMetDC/ODC this region is followed by the hinge region. Previous studies suggest that the hinge mediates domain interactions in the AdoMetDC/ODC complex [14].

The more conserved αβ-slice of PfAdoMetDC contains the more shorter and more conserved inserts 1 and 2. They are therefore predicted to be more important for the PfAdoMetDC domain than the remainder of the bifunctional complex. Deletion mutagenesis of a region encompassing insert 3 severely compromised PfAdoMetDC activity, but had no impact on bifunctional complex formation [14]. This is in agreement with the model, where insert 3 is predicted to occur on the edge opposite to the predicted dimerization edge of PfAdoMetDC (Figs. 1 and 3). However, this deletion was conducted prior to any investigation into the structure of PfAdoMetDC, and based on a previously published alignment, which predicted only one large insert for PfAdoMetDC [12]. The present study reveals that there are three inserts, therefore this deletion would have removed part of the PfAdoMetDC core structure and affected enzyme activity (helices 6,7 and 8, β-strand 9).

The model backbone RMSD (1.85 Å) indicates a satisfactory model that can be used to guide mutagenesis and related studies. Deviations as large as 1.5 Å can be expected for target-template sequence identities between 50 and 90% [38]. Most residues adopt allowed backbone angles, however long minimizations caused more residues to move into less favored conformations. This was also observed for the human template, and is considered to be an artifact of the energy function. It is known that once minimization has removed the worst violations, further minimization only results in the accumulation of small errors [38]. The residues in completely disallowed regions occur mostly in loops, where greater flexibility is expected (Fig. 4). β-strands 10 and 11 are in contact with the more diverged helices 8 and 9, which may explain their poorer superimposition with the templates. The absence of a model counterpart for human helix 5 may be due to the substitution of a proline residue found in the human template, adding increased flexibility. The corresponding structure for the potato template is also unresolved, and thus could not contribute to modeling. The extra helices 10 and 11 could only be modeled on the potato template, which is helical in this region, since the human template is unresolved [17,23]. Due to the lack of definitive knowledge regarding interacting regions within the bifunctional complex and the difficulties of modeling protein–protein interactions from homology models, no dimerization of PfAdoMetDC was attempted.

The active site region of the model and templates are highly conserved. The few substituted active site residues compared to the human enzyme are near enough to the ligand that they could allow for parasite-specific inhibition. The model replicates interactions observed between the human enzyme and the substrate. The orientation of MeAdoMet within the active site was similar for both the model and human structure. Gly3 replacing His5 *hum* may explain why Tris is observed to inhibit the human enzyme [39], but not the malaria enzyme [13]. Tris has been resolved in various crystal structures of the human enzyme and it has been suggested that His5 *hum* forms weak hydrogen bonds with the molecule [18,40], whereas Gly3 in the model provides no means to interact with Tris. All other residues suggested to interact with Tris are replicated in the model. His5 *hum* therefore may be more important than previously suggested for Tris inhibition in the human enzyme. The lack of Tris inhibition in the *P. falciparum* enzyme might further indicate that parasite-specific inhibitors could be found. Docking studies are underway to further determine the lack of Tris inhibition.

The sulfonium-methyl cavity suggests why inhibitors, which lack a positive charge corresponding to $S^+$, are less effective against AdoMetDC [41,42]. Acidic residues in the active site that may be required for this interaction have yet to be identified [23]. Most of these residues in the human enzyme form hydrogen bonds with the substrate analogue, and are therefore less likely candidates for this interaction. This leaves Glu11 *hum*, which lines this cavity as the only other residue that could interact with the positive charge. Glu11 *hum* is also required for processing [19], and the conservative mutation Glu11Asp results in inhibition of human AdoMetDC processing by putrescine [16]. Therefore, it is difficult to test this hypothesis using conventional replacement mutagenesis. In the human enzyme this cavity is occupied by two water molecules, which may possibly mediate the interaction between the sulfonium atom and Glu11 *hum*.

The processing and activity of certain AdoMetDCs is stimulated by putrescine, but not that of *P. falciparum* [13]. The modeling results suggest that a network of charged residues is conserved in *P. falciparum* that was previously observed in both human and potato AdoMetDC [22] (Fig. 6). Thus it appears that *P. falciparum* could have a similar transduction mechanism for putrescine-like effects, despite a lack of observable putrescine stimulation [13]. This network is not conserved in all species, however. Lys80 *hum* is replaced by Ile in *L. donovani*, *T. cruzi* and *T. brucei*, whereas Glu178 *hum* is replaced by Ser. *T. cruzi* exhibits stimulation of enzyme activity by putrescine, albeit at significantly higher concentrations, and by an apparently different mechanism of increasing $V_{max}$ instead of lowering $K_m$ [43]. Therefore it appears that for certain parasites the lack of putrescine stimulation may be due to the partial loss of residues needed to transmit the charge effect.

Other residues apparently required for putrescine-binding are absent in species not affected by putrescine. In PfAdoMetDC these residues are replaced by basic or non-polar residues (Table 2). The results indicate the Arg11, which connects with the charge network occupies one terminal of the putrescine site, while at the other terminal (not connected to the network) is occupied by Lys15 and Lys215. Any interaction with putrescine is therefore expected to be unfavorable due to repulsion between the amine ends of putrescine and these residues. Furthermore, these residues might be assuming the function of putrescine. This has already been suggested for potato [22], where Arg18 *pot*, Arg114 *pot* and other residues occupy the region of the putrescine terminals, and in *T. cruzi* where mutating the corresponding residue abolishes activity [44]. This is confirmed in *P. falciparum* where replacing Arg11 with Leu results in 90% loss of activity, and marginal processing. Therefore it is suggested that Arg11 simulates the role of putrescine in PfAdoMetDC to give a constitutively active enzyme, similar to potato AdoMetDC [22].

Docking putrescine in a chimeric model with a binding site more like the human enzyme gave a more favorable binding energy. The orientation of the best conformations within the chimeric model was similar to the human template. In the chimeric model the 11-RVVIK-15 motif of a β-strand is replaced by 11-LVEIW-15. The R × V × K motif forms part of a β-strand (β-strand 1, Fig. 2), with the side chains orientated towards the region occupied by putrescine. This motif is in line with putrescine in the human structure and chimeric model. The R × V × K motif is therefore suggested to be the most important set of residues for simulating putrescine, with Val13 substituting for the aliphatic putrescine backbone. This is supported by mutating Lys15 (K of R × V × K) to Ala, which results in about 50% decreased activity. A similar loss of activity is observed for Lys215Ala, predicted to occupy the other end of the lost putrescine-binding site together with Lys15. Lys215 occurs in a region of low sequence identity (in the region of β-sheet 9, Fig. 2), thus supporting the alignment used for modeling. Lys15 and Lys215 therefore appear to function together as one amine terminal of putrescine in PfAdoMetDC. Furthermore, the *in silico* simulations suggest the malarial enzyme can be converted to a putrescine stimulated-enzyme through suitable engineering. Further analysis of this mechanism is under way.

## 5. Conclusion

This study reveals a number of novel parasite-specific properties of *P. falciparum* AdoMetDC discovered as a result of molecular modeling. These properties include the presence of parasite-specific inserts, protein–protein contacts, active site residue substitutions, the lack of stimulation by putrescine, and the lack of inhibition by Tris. The diversity and number of these properties warrant further investigation of PfAdoMetDC as a therapeutic target. Furthermore, the model can guide further experimental investigations that may lead to the discovery of parasite-specific inhibitors.

## Acknowledgments

This material is based on work supported by the National Research Foundation (NRF) of South Africa, the Medical Research Council of South Africa, the University of Pretoria, the Deutsche Forschungsgemeinschaft (WA 395/10-3) and the German Scientific and Technological Cooperation with the Republic of South Africa, funded in part by the South African NRF and the International Bureau of the BMBF of Germany (project code: 39.6.G0B.5.A). Any opinion, findings and conclusions or recommendations expressed in this material are those of the author(s) and therefore the NRF does not accept any liability in regard thereto.

## References

[1] J. Breman, The ears of the hippopotamus: manifestations, determinants, and estimates of the malaria burden, Am. J. Trop. Med. Hyg. 64 (Suppl. 1/2) (2001) 1–11.

[2] K. Igarashi, I. Sakamoto, N. Goto, K. Kashiwagi, R. Honma, S. Hirose, Interaction between polyamines and nucleic acids or phospholipids, Arch. Biochem. Biophys. 219 (2) (1982) 438–443.

[3] C.W. Tabor, H. Tabor, Methionine adenosyltransferase (*S*-adenosylmethionine synthetase) and *S*-adenosylmethionine decarboxylase, Adv. Enzymol. Relat. Areas Mol. Biol. 56 (1984) 251–282.

[4] T. Byers, B. Ganem, A. Pegg, Cytostasis induced in L1210 murine leukaemia cells by the *S*-adenosyl-L-methionine decarboxylase inhibitor 5'-([(Z)-4-amino-2-butenyl]methylamino)-5'-deoxyadenosine may be due to hypusine depletion, Biochem. J. 287 (Pt 3) (1992) 717–724.

[5] T.L. Byers, R.S. Wechter, R.H. Hu, A.E. Pegg, Effects of the *S*-adenosylmethionine decarboxylase inhibitor, 5'-([(Z)-4-amino-2-butenyl]methylamino)-5'-deoxyadenosine, on cell growth and polyamine metabolism and transport in chinese hamster ovary cell cultures, Biochem. J. 303 (Pt 1) (1994) 89–96.

[6] S. Mller, E. Liebau, R. Walter, R. Krauth-Siegel, Thiol-based redox metabolism of protozoan parasites, Trends Parasitol. 19 (7) (2003) 320–328.

[7] O. Heby, S. Roberts, B. Ullman, Polyamine biosynthetic enzymes as drug targets in parasitic protozoa, Biochem. Soc. Trans. 31 (2) (2003) 415–419.

[8] L.J. Marton, A.E. Pegg, Polyamines as targets for therapeutic intervention, Annu. Rev. Pharmacol. Toxicol. 35 (1995) 55–91.

[9] J.E. Seely, H. Ps, A.E. Pegg, Measurement of the number of ornithine decarboxylase molecules in rat and mouse tissues under various physiological conditions by binding of radiolabelled alpha-difluoromethylornithine, Biochem. J. 206 (2) (1982) 311–318.

[10] C.C. Wang, molecular mechanisms and therapeutic approaches to the treatment of African trypanosomiasis, Annu. Rev. Pharmacol. Toxicol. 35 (1995) 93–127.

[11] S. Mller, G.H. Coombs, R.D. Walter, targeting polyamines of parasitic protozoa in chemotherapy, Trends Parasitol. 17 (5) (2001) 242–249.

[12] S. Müller, A. Da'dara, K. L´uersen, C. Wrenger, R. Das Gupta, R. Madhubala, R.D. Walter, In the human malaria parasite emPlasmodium falciparumem, polyamines are synthesized by a bifunctional ornithine decarboxylase, *S*-adenosylmethionine decarboxylase, J. Biol. Chem. 275 (11) (2000) 8097–8102.

[13] C. Wrenger, K. Lüersen, T. Krause, S. Müller, R.D. Walter, The *emPlasmodium falciparumem* bifunctional ornithine decarboxylase, *S*-adenosyl-L-methionine decarboxylase, enables a well balanced polyamine synthesis without domain-domain interaction, J. Biol. Chem. 276 (32) (2001) 29651–29656.

[14] L. Birkholtz, C. Wrenger, F. Joubert, G. Wells, R. Walter, A. Louw, Parasite-specific inserts in the bifunctional *S*-adenosylmethionine decarboxylase/ornithine decarboxylase of *Plasmodium falciparum* modulate catalytic activities and domain interactions, Biochem. J. 377 (Pt 2) (2004) 439–448.

[15] R.R. Allen, J.P. Klinman, Stereochemistry and kinetic isotope effects in the decarboxylation of *S*-adenosylmethionine as catalyzed by the pyruvoyl enzyme, *S*-adenosylmethionine decarboxylase, J. Biol. Chem. 256 (7) (1981) 3233–3239.

[16] H. Xiong, B.A. Stanley, A.E. Pegg, Role of cysteine-82 in the catalytic mechanism of human *S*-adenosylmethionine decarboxylase, Biochemistry 38 (8) (1999) 2462–2470.

[17] J.L. Ekstrom, I.I. Mathews, B.A. Stanley, A.E. Pegg, S.E. Ealick, The crystal structure of human *S*-adenosylmethionine decarboxylase at 2.25 Åresolution reveals a novel fold, Struct. Fold Des. 7 (5) (1999) 583–595.

[18] J.L. Ekstrom, W.D. Tolbert, H. Xiong, A.E. Pegg, S.E. Ealick, Structure of a human *S*-adenosylmethionine decarboxylase self-processing ester intermediate and mechanism of putrescine stimulation of processing as revealed by the H243A mutant, Biochemistry 40 (32) (2001) 9495–9504.

[19] B.A. Stanley, A.E. Pegg, Amino acid residues necessary for putrescine stimulation of human *S*-adenosylmethionine decarboxylase proenzyme processing and catalytic activity, J. Biol. Chem. 266 (28) (1991) 18502–18506.

[20] M.A. Hoyt, L.J. Williams-Abbott, J.W. Pitkin, R.H. Davis, Cloning and expression of the *S*-adenosylmethionine decarboxylase gene of Neuro-

spora crassa and processing of its product, Mol. Gen. Genet. 263 (4) (2000) 664–673.
[21] H. Xiong, B.A. Stanley, B.L. Tekwani, A.E. Pegg, Processing of mammalian and plant *S*-adenosylmethionine decarboxylase proenzymes, J. Biol. Chem. 272 (45) (1997) 28342–28348.
[22] E.M. Bennett, J.L. Ekstrom, A.E. Pegg, S.E. Ealick, Monomeric *S*-adenosylmethionine decarboxylase from plants provides an alternative to putrescine stimulation, Biochemistry 41 (49) (2002) 14509–14517.
[23] W.D. Tolbert, J.L. Ekstrom, I.I. Mathews, P. Kapoor, A.E. Pegg, S.E. Ealick, The structural basis for substrate specificity and inhibition of human *S*-adenosylmethionine decarboxylase, Biochemistry 40 (32) (2001) 9484–9494.
[24] J.D. Thompson, T.J. Gibson, F. Plewniak, F. Jeanmougin, D.G. Higgins, The clustalx windows interface: flexible strategies for multiple sequence alignment aided by quality analysis tools, Nucleic Acids Res. 25 (24) (1997) 4876–4882.
[25] T.L. Bailey, C. Elkan, Fitting a mixture model by expectation maximization to discover motifs in biopolymers, Proc. Int. Conf. Intell. Syst. Mol. Biol. 2 (1994) 28–36.
[26] A. Šali, T.L. Blundell, Comparative protein modelling by satisfaction of spatial restraints, J. Mol. Biol. 234 (3) (1993) 779–815.
[27] M.A. Marti-Renom, A.C. Stuart, A. Fiser, R. Sánchez, F. Melo, A. Šali, Comparative protein structure modeling of genes and genomes, Annu. Rev. Biophys. Biomol. Struct. 29 (2000) 291–325.
[28] A. Fiser, R.K. Do, A. Šali, Modeling of loops in protein structures, Protein Sci. 9 (9) (2000) 1753–1773.
[29] G.N. Ramachandran, C. Ramakrishnan, V. Sasisekharan, Stereochemistry of polypeptide chain configurations, J. Mol. Biol. 7 (1963) 95–99.
[30] A. Morris, M. MacArthur, E. Hutchinson, J. Thornton, Stereochemical quality of protein structure coordinates, Proteins 12 (4) (1992) 345–364.
[31] A.C. Wallace, R.A. Laskowski, J.M. Thornton, Ligplot: a program to generate schematic diagrams of protein–ligand interactions, Protein Eng. 8 (2) (1995) 127–134.
[32] Accelrys Inc., Cerius2 4. 6, Accelrys, Inc., San Diego, 2001.
[33] W. Kabsch, C. Sander, Dictionary of protein secondary structure: pattern recognition of hydrogen-bonded and geometrical features, Biopolymers 22 (12) (1983) 2577–2637.
[34] L. Birkholtz, F. Joubert, A. Neitz, A. Louw, Comparative properties of a three-dimensional model of *Plasmodium falciparum* ornithine decarboxylase, Proteins 50 (3) (2003) 464–473.
[35] E. Hafner, C. Tabor, H. Tabor, Mutants of *Escherichia coli* that do not contain 1,4-diaminobutane (putrescine) or spermidine, J. Biol. Chem. 254 (24) (1979) 12419–12426.
[36] M. Bradford, A rapid and sensitive method for the quantitation of microgram quantities of protein utilizing the principle of protein–dye binding, Anal. Biochem. 72 (1976) 248–254.
[37] B. Rost, Twilight zone of protein sequence alignments, Protein Eng. 12 (2) (1999) 85–94.
[38] E. Krieger, S. Nabuurs, G. Vriend, Homology modelling, Meth. Biochem. Anal. 44 (2003) 509–523.
[39] A. Pegg, H. Williams-Ashman, On the role of *S*-adenosylmethionine in the Biosynthesis of spermidine by rat prostate, J. Biol. Chem. 244 (1969) 682–693.
[40] W.D. Tolbert, Y. Zhang, S.E. Cottet, E.M. Bennett, J.L. Ekstrom, A.E. Pegg, S.E. Ealick, Mechanism of human *S*-adenosylmethionine decarboxylase proenzyme processing as revealed by the structure of the S68A mutant, Biochemistry 42 (8) (2003) 2386–2395.
[41] M. Pankaskie, M.M. Abdel-Monem, Inhibitors of polyamine biosynthesis. 8. Irreversible inhibition of mammalian *S*-adenosyl-L-methionine decarboxylase by substrate analogues, J. Med. Chem. 23 (2) (1980) 121–127.
[42] A.E. Pegg, G. Jacobs, Comparison of inhibitors of *S*-adenosylmethionine decarboxylase from different species, Biochem. J. 213 (2) (1983) 495–502.
[43] L.N. Kinch, J.R. Scott, B. Ullman, M.A. Phillips, Cloning and kinetic characterization of the *Trypanosoma cruzi*, Mol. Biochem. Parasitol. 101 (1/2) (1999) 1–11.
[44] T. Clyne, L. Kinch, M. Phillips, Putrescine activation of *Trypanosoma cruzi S*-adenosylmethionine decarboxylase, Biochemistry 41 (44) (2002) 13207–13216.